Synthesis and Characterization of Pyrido[3,4-*b*]pyrazine-Based Low-Bandgap Copolymers for Bulk Heterojunction Solar Cells

Mao-Chuan Yuan, Mao-Yuan Chiu, Chien-Ming Chiang, and Kung-Hwa Wei*

Department of Materials Science and Engineering, National Chiao Tung University, 300 Hsinchu, Taiwan, ROC

Received March 8, 2010; Revised Manuscript Received June 16, 2010

ABSTRACT: We have used Stille polycondensation to prepare a series of low-bandgap copolymers, **P1**−**P4**, by conjugating the electron-accepting pyrido[3,4-*b*]pyrazine (**PP**) moieties with the electron-rich benzo[1,2-*b*:3,4-*b′*]dithiophene (**BDT**) or cyclopentadithiophene (**CPDT**) units. **P1** and **P3** are based on **PP** and **BDT** units while **P2** and **P4** are based on **PP** and **CPDT** units. All of these polymers exhibited excellent thermal stability and sufficient energy offsets for efficient charge transfer and dissociation, as determined through thermogravimetric analyses and cyclic voltammetry, respectively. The bandgaps of the polymers could be tuned in the range 1.46−1.60 eV by using the two different donors, which have different electron-donating abilities. The three-component copolymers, **P3** and **P4**, incorporating the thiophene and bithiophene segments, respectively, absorbed broadly, covering the solar spectrum from 350 to 800 nm. The morphologies of the blends of **P3** and **P4** with [6,6]-phenyl-C_{70}-butyric acid methyl ester ($PC_{70}BM$) were more homogeneous than those of **P1** and **P2**; in addition, devices incorporating the **P3** and **P4** blends exhibited superior performance. The best device performance resulted from an active layer containing the **P4**:$PC_{70}BM$ blend; the short-circuit current was 10.85 mA cm^{-2} and the power conversion efficiency was 3.15%.

Introduction

In recent years, conjugated polymers possessing extended delocalized π-electron systems have been studied extensively for their application in bulk heterojunction (BHJ) solar cells, which generally feature a polymeric donor and a fullerene-based acceptor.[1−4] Regioregular polythiophene derivatives have been widely investigated for BHJs because of their highly crystallizable state, leading to good light harvesting in the visible spectrum and excellent carrier mobility. Power conversion efficiencies (PCEs) of up to 5% have been achieved when using poly(3-hexylthiophene)/[6,6]-phenyl-C_{61}-butyric acid methyl ester (P3HT/PCBM) composites as the photoactive layer.[5−8] Nevertheless, the efficiency of this system is difficult to improve because of the limited absorption range of P3HT, which absorbs photons only at wavelengths less than 650 nm and merely ca. 22% of the absorbed photons from sunlight.[9] In attempts to harvest more photons and further improve the efficiencies of polymer solar cells (PSCs), several conjugated polymers featuring electron donor−acceptor (D−A) units in main chain−conjugated configurations[10−14] and side chain−attached architectures[15−19] have been developed because of their tunable electronic properties, ambipolar charge transport abilities, and enlarged spectral absorption ranges. Low-bandgap D−A polymers have attracted considerable attention because their absorption ranges are broader than that of P3HT; for example, the presence of intramolecular charge transfer (ICT) bands arising from push/pull interactions between the D and A units can extend the absorption into the near-infrared (NIR) region of the solar spectrum.[20−26] The properties of D−A polymers can be tuned by varying the structures of the D and A units.

Several D−A conjugated polymers based on electron-accepting pyrido[3,4-*b*]pyrazine (**PP**) moieties have been described previously.

These **PP**-containing polymers have displayed higher electron-accepting abilities relative to that of quinoxaline-containing polymers because the former feature more electron-withdrawing nitrogen atoms in the fused ring.[27−29] The poly(pyridopyrazine-phenylene) polymer has been used in NIR light-emitting diodes;[30] another polymer, in which the **PP** moieties were conjugated with thiophene/fluorene units, has been used in field-effect transistors, with hole mobilities of up to 4.4×10^{-3} cm^2 V^{-1} s^{-1}.[31] To date, only a few PSCs prepared from **PP**-containing polymers have been investigated;[32−35] they have exhibited moderate PCEs (up to 1.1%)[34] because of their low molecular weights and/or poor solubility.

In this study, we used Stille polycondensation to prepare four **PP**-containing low-bandgap polymers of high molecular weight and exhibiting good solubility. The presence of octyloxyphenyl groups attached to the **PP** moieties increased the solubility and, thereby, extended the conjugation length of the synthesized polymers. Furthermore, because several low-bandgap polymers incorporating benzo[1,2-*b*:3,4-*b′*]dithiophene (**BDT**)[21,36,37] and cyclopentadithiophene (**CPDT**)[38−41] units in their backbones exhibit high electron-donating ability and good performance when applied in PSCs, we incorporated these two electron-rich donors into our polymer backbones by conjugating them with electron-withdrawing **PP** moieties. Using this approach allowed us to fine-tune the absorption spectra and energy levels because of the modulated ICT strength between the **PP** moieties and the **BDT**/**CPDT** units, thereby leading to PSCs exhibiting varied photovoltaic performance. Because our synthesized polymers, **P1** and **P2** absorb too little in the visible range, where the radiated intensity of photons in the solar spectrum was quite high, due to their low-bandgap characteristics; therefore, we synthesized the three-component random copolymers **P3** and **P4**, through further incorporation of thiophene/bithiophene segments, to extend the light-harvesting range. **P3** and **P4** displayed very broad absorption ranges, covering the solar spectrum from the

*Corresponding author. E-mail: khwei@mail.nctu.edu.tw.

visible to a significant portion of the NIR region. Thus, we expected the performance of the devices prepared from **P3** and **P4** to be significantly improved.

Experimental Section

Materials. 1-Bromo-3-octyloxybenzene (**1**),[42] 1,2-bis(3-octyloxyphenyl)ethane-1,2-dione (**2**),[42] 3,4-diamino-2,5-dibromopyridine (**3**),[27] benzo[1,2-*b*:4,5-*b*′]dithiophene-4,8-dione (**4**),[21] 1,5-bis(trimethylstannyl)-4,8-dioctylbenzo[1,2-*b*:4,5-*b*′]dithiophene (**M2**),[21] 4,4-bis(2-ethylhexyl)-2,6-bis(trimethylstannyl)-4*H*-cyclopenta[2,1-*b*:3,4-*b*′]-dithiophene (**M3**),[38] and 5,5′-dibromo[2,2′]-bithiophene (**M5**)[44] were prepared according to reported procedures. [6,6]-Phenyl-C_{70}-butyric acid methyl ester ($PC_{70}BM$) was purchased from Nano-C. 2,5-Dibromothiophene (**M4**) and all other reagents were used as received without further purification, unless stated otherwise.

Measurements and Characterization. ^1H and ^{13}C NMR spectra were recorded using a Varian UNITY 300 MHz spectrometer. Mass spectra were obtained using a JEOL JMS-HX 110 spectrometer. Differential scanning calorimetry (DSC) was performed using a Perkin−Elmer Pyris 1 unit operated at heating and cooling rates of 20 and 40 °C min^{-1}, respectively; the glass transition temperatures (T_g) were determined from the second heating scan. Thermogravimetric analysis (TGA) was undertaken using a TA Instruments Q500; the thermal stabilities of the samples were determined under a N_2 atmosphere by measuring their weight losses while heating at a rate of 20 °C min^{-1}. Size exclusion chromatography (SEC) was performed using a Waters chromatography unit interfaced with a Waters 1515 differential refractometer; polystyrene was the standard and THF was the eluant. UV−Vis spectra of dilute chloroform solutions (1×10^{-5} M) were measured using a Hitachi U-4100 spectrophotometer. Solid films for UV−Vis analysis were obtained by spin-coating dichlorobenzene (DCB) solutions of the copolymers (10 mg mL^{-1}) onto quartz substrates. Cyclic voltammetry (CV) was performed using a BAS 100 electrochemical analyzer operated at a scan rate of 50 mV s^{-1}; the solvent was anhydrous acetonitrile containing 0.1 M tetrabutylammonium hexafluorophosphate ($TBAPF_6$) as the supporting electrolyte. The potentials were measured against a Ag/Ag$^+$ (0.01 M AgNO$_3$) reference electrode; ferrocene/ferrocenium ion (Fc/Fc$^+$) was used as the internal standard. The onset potentials were determined from the intersection of two tangents drawn at the rising and background currents of the cyclic voltammogram. Topographic images of the copolymer:$PC_{70}BM$ films (surface area: 5×5 μm^2) were obtained through atomic force microscopy (AFM) in the tapping mode under ambient conditions using a Digital Nanoscope IIIa instrument. Transmission electron microscopy (TEM) images of the copolymer:$PC_{70}BM$ films were recorded using a FEI T12 TEM operating at 120 KeV. The thickness of the active layer was measured using a Veeco Dektak 150 surface profiler. Hole-only mobility measurements were performed using the device structure of ITO/PEDOT:PSS/ **P1−P4**:$PC_{70}BM$ (1:4, w/w)/Au. The hole mobilities of the blends were determined by fitting the dark $J−V$ curve into the space-charge-limited current (SCLC) model,[17,43] based on the equation

$$J = \frac{9}{8}\varepsilon_0\varepsilon_r\mu_h\frac{V^2}{L^3}$$

Here ε_0 is the permittivity of free space, ε_r is the dielectric constant of the material, μ_h is the hole mobility, V is the voltage drop across the device, and L is the thickness of the active layer.

Fabrication and Characterization of Photovoltaic Devices. Indium tin oxide (ITO) coated glass substrates were cleaned stepwise in detergent, water, acetone, and isopropyl alcohol (ultrasonication; 20 min each) and then dried in an oven for 1 h; subsequently, the substrates were treated with UV ozone for

10 min prior to use. A thin layer (ca. 20 nm) of poly(ethylenedioxythiophene):poly(styrenesulfonate) (PEDOT:PSS, Baytron P VP AI 4083) was spin-coated at 5000 rpm onto the ITO substrates. After baking at 140 °C for 20 min in air, the substrates were transferred into a N_2-filled glovebox. The copolymers **P1−P4** were codissolved with $PC_{70}BM$ in DCB (weight ratio, 1:4; total concentration, 25 mg mL^{-1}) and stirred continuously for 12 h at 50 °C. The photoactive layer was obtained by spin-coating the blend solution onto the ITO/PEDOT:PSS surface at 800 rpm for 60 s without further special treatment. The thicknesses of the photoactive layers were ca. 75−95 nm. Finally, an Al layer (100 nm) was thermally evaporated through a shadow mask under a vacuum of less than 1×10^{-6} Torr. The effective layer area of one cell was 0.04 cm^2. The current density−voltage ($J−V$) characteristics were measured using a Keithley 236 source-meter. The photocurrent was measured under simulated AM 1.5 G irradiation at 100 mW cm^{-2} using a Xe lamp−based Newport 66902 150W solar simulator. The spectrum of the solar simulator was calibrated using a PV-measurement (PVM-154) monosilicon solar cell (NREL calibrated) to minimize spectral mismatch; a silicon photodiode (Hamamatsu S1133) was employed to check the uniformity of the exposed area. External quantum efficiency (EQE) was measured using a system established by Optosolar, Inc. Monochromatic light was created from a 500-W Xe lamp source passing through a monochromator. The photocurrent of the device was detected using a lock-in amplifier under short-circuit conditions by illuminating the monochromatic incident beam. A calibrated mono silicon diode exhibiting a response at 350−1000 nm was used as a reference.

5,8-Dibromo-2,3-bis(3-octyloxyphenyl)pyrido[3,4-*b*]pyrazine (M1). A mixture of **1** (0.91 g, 1.95 mmol), **2** (0.52 g, 1.95 mmol), and acetic acid (20 mL) was heated at 50 °C for 4 h under N_2. The mixture was poured into water (100 mL) and the resulting precipitate collected by filtration. The crude product was purified through column chromatography (EtOAc/hexane, 1:10) and then recrystallized twice from ethanol to afford **M1** (0.91 g, 67%) as a yellow solid. ^1H NMR (300 MHz, CDCl$_3$): δ 0.87−0.91 (m, 6H), 1.30−1.44 (m, 20H), 1.69−1.78 (m, 4H), 3.83−3.89 (m, 4H), 6.95−6.99 (m, 2H), 7.15−7.28 (m, 6H), 8.76 (s, 1H). ^{13}C NMR (75 MHz, CDCl$_3$): δ 14.1, 22.7, 26.0, 29.0, 29.2, 29.3, 31.8, 68.1, 115.6, 115.7, 117.0, 117.3, 120.1, 122.4, 122.5, 129.5, 135.8, 138.3, 138.4, 142.4, 146.2, 147.2, 156.1, 158.2, 159.1, 159.2. MS (*m/z*): [M]$^+$ calcd for $C_{35}H_{43}Br_2N_3O_2$, 697.1; found, 697. Anal. Calcd for $C_{35}H_{43}Br_2N_3O_2$: C, 60.27; H, 6.21; N, 6.02. Found: C, 60.32; H, 6.61; N, 6.05.

Alternating Copolymer P1. A mixture of **M1** (100 mg, 0.143 mmol), **M2** (111 mg, 0.143 mmol), and tri(*o*-tolyl)phosphine (3.6 mg, 8.0 mol %) was dissolved in dry chlorobenzene (CB) (3 mL) and degassed for 15 min. Tris(dibenzylideneacetone)-dipalladium (2.6 mg, 2.0 mol %) was added under N_2 and then the reaction mixture was heated at 130 °C for 36 h. After cooling to room temperature, the solution was added dropwise into methanol (100 mL). The crude polymer was collected, dissolved in chlorobenzene, and reprecipitated in methanol. The solid was washed with methanol, acetone, and chloroform in a Soxhlet apparatus. The chloroform solution was concentrated and then added dropwise into methanol. Finally, the polymer was collected and dried under vacuum to give **P1** (113 mg, 80%). ^1H NMR (300 MHz, CDCl$_3$): δ 0.76−2.10 (m, 60H), 3.67−4.41 (m, 8H), 6.84−7.80 (m, 10H), 8.84 (br, 1H). Anal. Calcd: C, 74.42; H, 8.29; N, 4.27. Found: C, 73.56; H, 8.02; N, 4.23.

Alternating Copolymer P2. Using a polymerization procedure similar to that described above for **P1**, a mixture of **M1** (120 mg, 172 mmol) and **M3** (125 mg, 172 mmol) in dry CB (3 mL) was copolymerized to give **P2** (110 mg, 68%). ^1H NMR (300 MHz, CDCl$_3$): δ 0.62−0.67 (m, 12H), 0.75−1.01 (m, 22H), 1.15−1.45 (m, 22H), 1.66−2.08 (m, 8H), 3.97 (br, 4H), 7.07 (br, 2H), 7.36−7.48 (m, 6H), 7.88 (s, 1H), 8.67 (s, 1H), 9.18 (s, 1H). Anal. Calcd: C, 76.63; H, 8.68; N, 4.47. Found: C, 72.26; H, 8.08; N, 4.11.

**Scheme 1. Synthetic Routes of the Monomers**
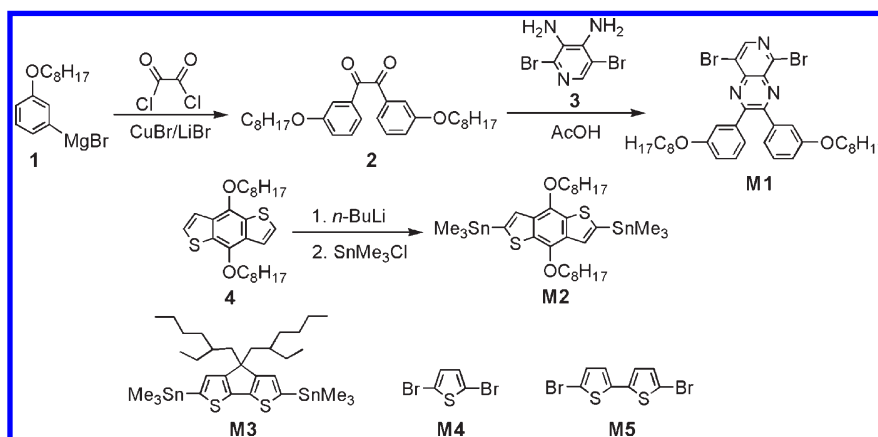
Alternating Copolymer P3. Using a polymerization procedure similar to that described above for **P1**, a mixture of **M1** (60.0 mg, 0.086 mmol), **M2** (133 mg, 0.172 mmol), and **M4** (20.8 mg, 0.086 mmol) in dry CB (2.8 mL) was copolymerized to give **P3** (106 mg, 82%). ^{1}H NMR (300 MHz, CDCl$_3$): δ 0.77−0.95 (m, 46H), 1.18−1.48 (m, 146H), 3.94−4.32 (m, 12H), 7.05−7.47 (m, 14H), 8.98 (br, 1H). Anal. Calcd: C, 72.32; H, 7.94; N, 2.78. Found: C, 72.00; H, 7.88; N, 2.87.

Alternating Copolymer P4. Using a polymerization procedure similar to that described above for **P1**, a mixture of **M1** (72.1 mg, 0.103 mmol), **M3** (151 mg, 0.206 mmol), and **M5** (33.5 mg, 0.103 mmol) in dry CB (2.8 mL) was copolymerized to give **P4** (108 mg, 70%). ^{1}H NMR (300 MHz, CDCl$_3$): δ 0.66−1.15 (m, 68H), 1.32−1.53 (m, 18H), 1.75−1.98 (m, 12H), 3.97−4.10 (m, 4H), 6.95−7.17 (m, 8H), 7.24−7.55 (m, 6H), 7.82 (br, 1H), 8.62 (s, 1H), 9.16 (s, 1H). Anal. Calcd: C, 74.20; H, 8.10; N, 2.79. Found: C, 73.57; H, 7.97; N, 2.81.

Results and Discussion

Synthesis and Characterization of the Copolymers. As indicated in Scheme 1, we prepared the symmetric 1,2-diketone **2** presenting two 3-octyloxyphenyl groups through a Grignard reaction between 3-octyloxyphenylmagnesium bromide (**1**) and oxalyl chloride in the presence of CuBr and LiBr. Condensation of **2** with the diamine **3** afforded the monomer **M1**; the distannyl monomer **M2** was prepared through dilithiation of compound **4** with *n*-BuLi, followed by quenching with trimethylstannyl chloride. With the monomers **M1**−**M5** in hand, we prepared the **PP**-based alternating/random copolymers **P1**−**P4** through Stille polycondensations using various feed molar ratios of the corresponding monomers (Scheme 2). **P1** and **P3**, which featured electron-donating **BDT** units, had weight-average molecular weights (M_w) of 398 and 563 kg mol^{-1}, respectively, and polydispersities of 2.65 and 2.54, respectively, as determined through gel permeation chromatography (GPC) using polystyrene standards. The donor moieties of the polymers **P2** and **P4** were highly coplanar fused **CPDT** units; their values of M_w were 101 and 89 kg mol^{-1}, respectively, with polydispersities of 1.65 and 1.79, respectively. The relatively high molecular weights of **P1** and **P3**, relative to those of **P2** and **P4**, presumably resulted from the high reactivity of the **BDT** moieties in their polymerization reactions. The solubility of the copolymers in various solvents was determined at a concentration of 5 mg/mL. We found that **P1** and **P3** were completely soluble in THF, CHCl$_3$, CB, or DCB at room temperature and became soluble in toluene at 60 °C; **P2** and **P4** were completely soluble in THF, CHCl$_3$, CB, DCB, or toluene at room temperature. We also synthesized

**Scheme 2. Synthetic Routes of the Copolymers.**[a]
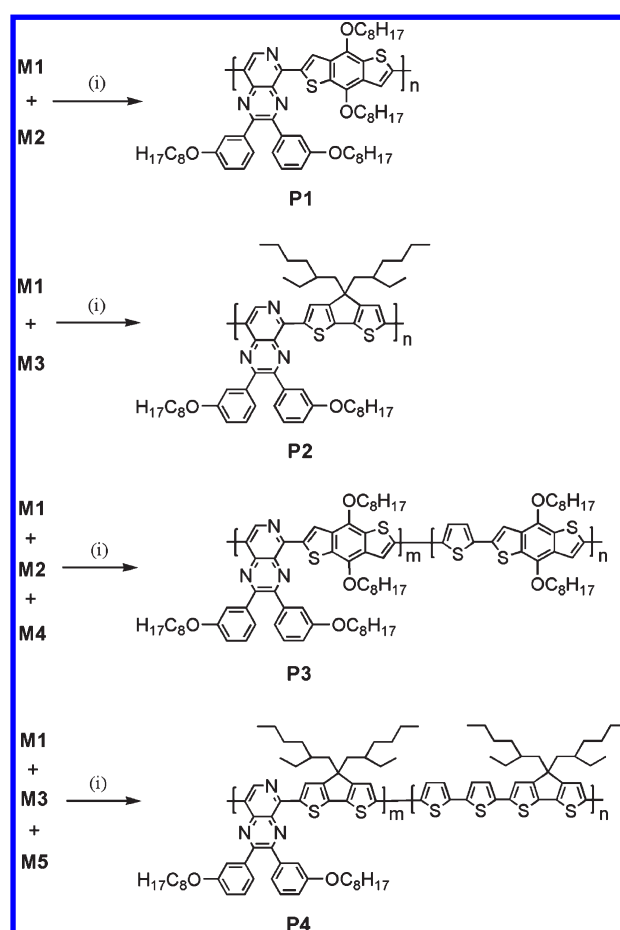
[a] Reagents: (i) Pd$_2$dba$_3$, tri(*o*-tolyl)phosphine, chlorobenzene.

nonsubstituted polymers through reacting the **PP** unit without any alkyl chain with the **BDT** or **CPDT** units, and both of them have insoluble precipitation in toluene, THF, CB or DCB. We characterized the synthesized monomers and polymers using ^{1}H and ^{13}C NMR spectroscopy, mass spectrometry, and elemental analysis. We estimated the copolymers' composition using the ratio of the integrated value of the proton peak on the **PP** unit (−N−CH−) to that of the proton peak on the thiophene/bithiophene units (thiophene-H) from their NMR spectra; the output composition (m:n) for **P3** and **P4** was 0.97:1 and 1:0.98, respectively, and they are very close to the feed ratios.
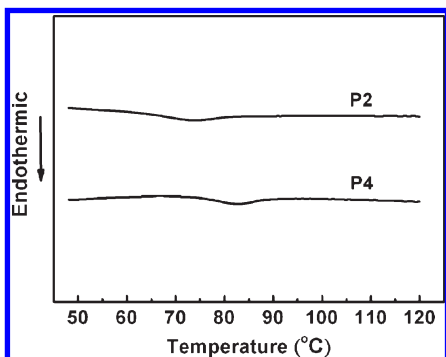
Figure 1. DSC traces of the copolymers **P2** and **P4**, recorded at a heating rate of 20 °C min^{-1} under a N$_2$ atmosphere.
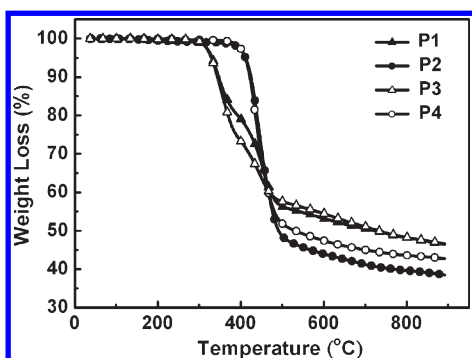
Figure 2. TGA thermograms of the copolymers **P1**–**P4**, recorded at a heating rate of 20 °C min^{-1} under a N$_2$ atmosphere.

**Table 1. Polymerization Data and Thermal Properties of the Copolymers**

	feed ratio					M_w (10^4)	M_n (10^4)	PDI	T_g (°C)	T_d (°C)
copolymer	M1	M2	M3	M4	M5					
P1	0.5	0.5				39.8	15.0	2.65	n.d.^{a}	332
P2	0.5		0.5			10.1	6.1	1.65	68	412
P3	0.25	0.5		0.25		56.3	22.1	2.54	n.d.^{a}	330
P4	0.25		0.5		0.25	8.9	5.0	1.79	77	410

^{a} Glass transition temperature was not detectable.

We investigated their thermal behavior through DSC analysis, which revealed no obvious thermal transitions for **P1** and **P3** in the temperature range from 40 to 300 °C; in contrast, **P2** and **P4** exhibited distinct glass transition temperatures (T_g) at 68 and 77 °C, respectively (Figure 1). Thus, **P1**–**P4** displayed amorphous properties. We attribute the slightly higher value of T_g obtained for **P4** to the presence in its backbone of the more rigid bithiophene segment, which presumably enhanced the chain rigidity[45] while reducing the number of the alkyl groups in the polymer chain. Figure 2 displays the TGA curves of these polymers. The 5% weight loss temperature (T_d) of each polymer was greater than 330 °C; such good thermal stability is an important prerequisite for a polymer's application to PSCs. Table 1 summarizes the molecular weights, polydispersities, and thermal properties of the polymers.

Photophysical Properties. Figure 3 presents absorption spectra of the copolymers **P1**–**P4**, recorded for both dilute (1 × 10^{-5} M) CHCl$_3$ solutions and solid films; Table 2 summarizes the spectral data. In solution, **P1** and **P2** displayed absorption peaks close to 400 nm that we assign to their localized π–π^* transition bands and at 668 and 776 nm, respectively, that we attribute to ICT interactions between
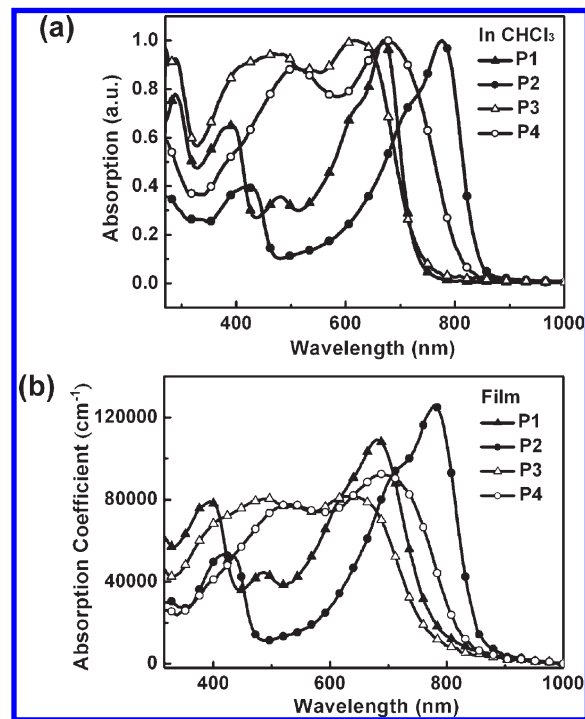
Figure 3. UV–vis absorption spectra of the copolymers **P1**–**P4** (a) in dilute chloroform solutions (1 × 10^{-5} M) (b) as solid films.

the **PP** acceptor moieties and the **BDT/CPDT** donor units. The absorption maximum of **P2** was red-shifted by ca. 108 nm, relative to that of **P1**, because of the stronger ICT effect in **P2** than that in **P1**, indicating that the fused **CPDT** unit has stronger electron-donating ability than does the **BDT** unit. The three-component copolymer **P3** exhibited two combined, but distinct, absorption bands of almost equal intensity, with absorption maxima at 468 and 616 nm, respectively. We attribute the higher-energy band to the absorption of the **BDT**-thiophene segment, consistent with reports of related polymers in the literature,[36] and the lower-energy band to ICT of the **BDT-PP** segment. The spectrum of **P3** exhibited an absorption maximum having a hypsochromic shift of ca. 50 nm relative to that of **P1** because the incorporation of the higher-energy **BDT**-thiophene segment shifted the absorption to the shorter wavelength region. **P4** exhibited similar optical properties as those of **P3**, with absorption maxima at 505 and 676 nm that we attribute to the **CPDT**-bithiophene and **CPDT-PP** segments, respectively. The absorption spectra of **P1**–**P4** in the solid state were similar to their corresponding solution spectra, with slight red shifts of ca. 6–18 nm of their absorption maxima, indicating there some intermolecular interactions occurred in their solid states. Figure 3 reveals that **P3** and **P4** absorbed broadly in the region 350–800 nm, extending from the visible to a portion of the NIR region of the solar spectrum; such an absorption is a desirable property for generating higher photocurrents in solar cells.

The optical bandgaps (E_g^{opt}) of **P1**–**P4**, estimated from the onsets of absorption in their solid films, were 1.58, 1.46, 1.60, and 1.49 eV, respectively. Generally, the incorporation of electron donating groups reduces the optical bandgaps by raising the energy levels of the highest occupied molecular orbital (HOMO).[46] We suspect that the optical bandgaps of **P2** and **P4** were lower than those of **P1** and **P3** because the incorporation of the more strongly electron-donating and highly coplanar **CPDT** units resulted in stronger ICT interactions when conjugated with the **PP** acceptors.[12,47]

**Table 2. Optical and Redox Properties of the Copolymers**

	absorption, λ_{max} (nm)		E_g^{opt} (eV)[a]	E_{onset}^{ox} (V)	E_{onset}^{red} (V)	HOMO (eV)[b]	LUMO (eV)[b]	E_g^{ec} (eV)[c]
	solution	film						
P1	668	680	1.58	0.42	1.48	5.22	3.32	1.90
P2	776	779	1.46	0.38	1.49	5.18	3.31	1.87
P3	468, 616	494, 634	1.60	0.40	1.52	5.20	3.28	1.92
P4	505, 676	529, 690	1.49	0.33	1.50	5.13	3.30	1.83

[a] Estimated from the onset wavelength absorptions of the solid films. [b] Calculated from the corresponding onset potentials. [c] Calculated form the difference between the onset potentials for oxidation and reduction.
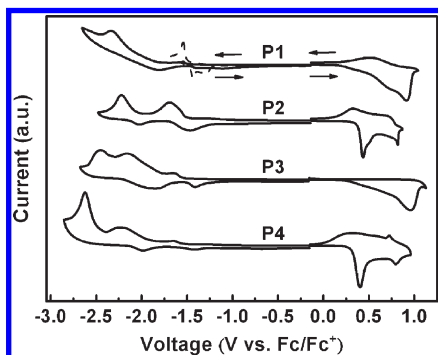
Figure 4. Cyclic voltammograms of the copolymers **P1**−**P4** as solid films.

Electrochemical Properties. We used CV to investigate the redox behavior of the copolymers and obtain their HOMO and lowest occupied molecular orbital (LUMO) energy levels. Figure 4 displays the electrochemical behavior of the copolymers as solid films; Table 2 summarizes the relevant data. All synthesized polymers exhibited partially reversible oxidations, except for **P3**, which underwent an irreversible oxidation. The onset potentials of **P1** and **P3** were 0.42 and 0.40 V, respectively, arising essentially from the oxidation of the electron-donating **BDT** units,[36] although the cyclic voltammograms revealed indistinct oxidation peaks of the **BDT** units intermixed in the hybrid oxidation region. **P2** and **P4** exhibited oxidation onsets of 0.38 and 0.33 V, respectively, resulting from the oxidation of the **CPDT** units.[40] In their reduction traces, **P1**−**P4** exhibited reversible reduction peaks, with similar onset potentials between −1.48 and −1.52 V, which we assign to reductions of the electron-accepting **PP** moieties; these values are comparable with those reported previously for other **PP**-containing copolymers.[27] On the basis of these onset potentials, we estimated the HOMO and LUMO energy levels according to the energy level of the ferrocene reference (4.8 eV below vacuum level).[23,48,55] Accordingly, the HOMO energy levels of **P1**−**P4** were 5.22, 5.18, 5.20, and 5.13 eV, respectively, implying that they varied with respect to the modulated ICT strengths resulting from the presence of the electron donors exhibiting various electron-donating abilities.[12,20,47] The LUMO energy levels of **P1**−**P4** were all located within a reasonable range (3.28−3.32 eV) and were significantly greater than that of PC$_{70}$BM (ca. 4.2 eV);[13,20] thus, we would expect efficient charge transfer/dissociation to occur in their devices.[13,49−51] In addition, the electrochemical bandgaps (E_g^{ec}) of **P1**−**P4**, estimated from the difference between the onset potentials for oxidation and reduction, were in the range 1.83−1.92 eV; i.e., they were slightly larger than their corresponding optical bandgaps. This discrepancy between the electrochemical and optical bandgaps presumably resulted from the exciton binding energies of the polymers[31] and/or the interface barrier for charge injection.[52]

Hole Mobility. Figure 5 displays the hole mobilities of the devices incorporating the **P1**−**P4**:PC$_{70}$BM blends with a
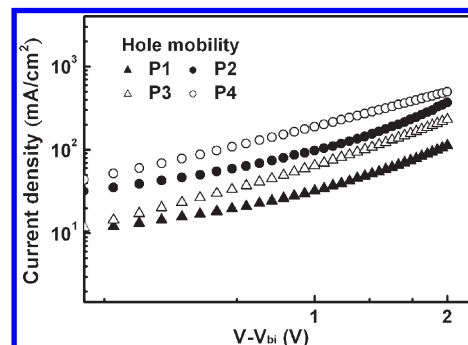

Figure 5. Dark J−V curves for the hole-dominated carrier devices incorporating the **P1**−**P4**:PC$_{70}$BM blends, each prepared at a blend ratio of 1:4 (w/w).
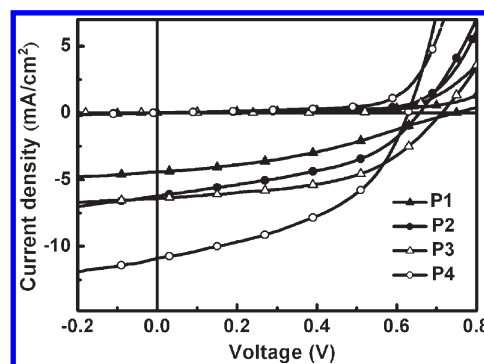
Figure 6. J−V characteristics of PSCs incorporating **P1**−**P4**:PC$_{70}$BM blends, each prepared at a blend ratio of 1:4 (w/w).

blend ratio of 1:4 (w/w). The hole mobilities of **P2** and **P4** blends were 1.67×10^{-4} and 2.36×10^{-4} cm^2 V^{-1} s^{-1}, respectively while that of **P1** and **P3** blends are 7.81×10^{-5} and 1.37×10^{-4} cm^2 V^{-1} s^{-1}, respectively. The fact that the hole mobility of the **P4**:PC$_{70}$BM blend being higher than that of **P1**−**P3** blends is probably due to the more homogeneous morphology of the **P4** blend.

Photovoltaic Properties. Next, we investigated the photovoltaic properties of the polymers in bulk heterojunction solar cells having the sandwich structure ITO/PEDOT:PSS/polymer:PC$_{70}$BM (1:4, w/w)/Al, where the photoactive layers had been spin-coated from dichlorobenzene solutions. Figure 6 presents the J−V curves of these PSCs; Table 3 summarizes the data. The devices prepared from **P1**−**P4**:PC$_{70}$BM blends exhibited open circuit voltages (V_{oc}) of 0.74, 0.66, 0.71, and 0.63 V, respectively; each value is related to the difference between the HOMO energy level of the polymer and the LUMO energy level of PC$_{70}$BM.[51] We suspect that the **P4** blend provided the lowest value of V_{oc} because of its relatively higher-lying HOMO energy level. The short-circuit current densities (J_{sc}) of the devices incorporating the **P3** and **P4** blends (6.40 and 10.85 mA cm^{-2}, respectively) were significantly greater than those of **P1** (4.69 mA cm^{-2})
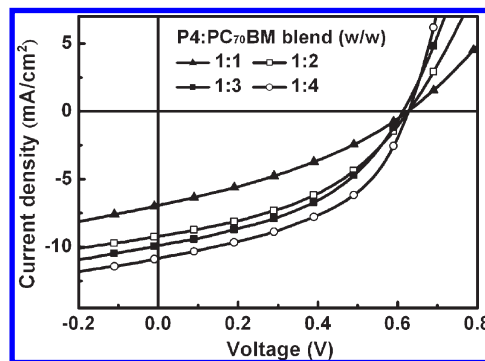
Table 3. Photovoltaic Properties of Polymer Solar Cells Incorporating P1−P4:$PC_{70}BM$ Blends Prepared at 1:4 Weight Ratios

polymer	thickness (nm)	V_{oc} (V)	J_{sc} (mA cm^{-2})	FF	PCE (%)
P1	95	0.74	4.69	34.5	1.20
P2	80	0.66	6.26	44.1	1.82
P3	92	0.71	6.41	51.7	2.35
P4	75	0.63	10.85	46.1	3.15
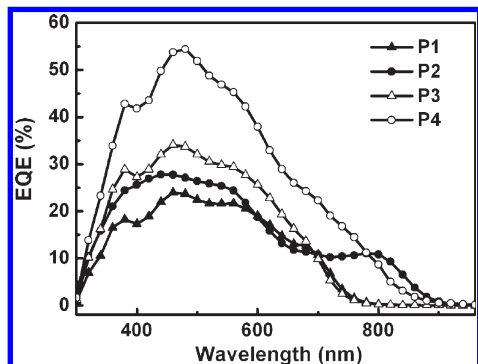
Figure 7. EQE curves of PSCs incorporating **P1−P4**:$PC_{70}BM$ blends, each prepared at a blend ratio of 1:4 (w/w).

and **P2** (6.26 mA cm^{-2}). Because the light-harvesting coverages of the former pair were significantly broader than those of the latter pair, more available photos from the solar radiation could be absorbed by **P3** and **P4**, thereby leading to higher photocurrents. The device incorporating the **P3** blend exhibited a value of V_{oc} of 0.71 V, a value of J_{sc} of 6.40 mA cm^{-2}, a fill factor (FF) of 0.517, and a PCE of 2.35%; the device featuring the **P4** blend displayed even greater performance, with values of V_{oc}, J_{sc}, FF, and PCE of 0.63 V, 10.85 mA cm^{-2}, 0.461, and 3.15%, respectively. Figure 7 displays the external quantum efficiency (EQE) curves of the devices incorporating the **P1−P4**:$PC_{70}BM$ blends at weight ratio of 1:4. These devices exhibited a significantly broad EQE responses extending from the visible to the NIR, with a maximum intensity ranging between 460 and 480 nm. We attribute their higher EQE responses in the visible region to the corresponding higher absorbance of the blend, resulted from both the intrinsic absorption of the polymer and the presence of a high content of $PC_{70}BM$, which also absorbs significantly at 400−500 nm. In contrast, these devices displayed relatively lower EQE responses at wavelengths above 700 nm because of the moderate absorbance of the polymer blend. The device of **P4** blend exhibited a higher EQE response than that of other polymer blends, with a maximum of 54% at 480 nm, corresponding to its higher photocurrent. The theoretical short-circuit current density obtained from integrating the EQE curve of the **P4** blend is 9.90 mA/cm^2, that is reasonably agreed to the measured J_{sc} of 10.85 mA/cm^2 AM 1.5G. For the **P1−P3** blends, the discrepancy between the theoretical and the measured J_{sc} is around 10%. To optimize the device performance of the most efficient polymer **P4**, devices of various compositions incorporating the **P4**:$PC_{70}BM$ blend were investigated. Figure 8 presents the J−V curves of the PSCs; Table 4 summarizes the data. The power conversion efficiencies of **P4** devices increased with the weight ratio of $PC_{70}BM$ owing to the enhanced photocurrent and fill factor. A high percentage (80%) of $PC_{70}BM$ was required in the **P4** blend to obtain such high efficiency. Similar phenomena have been observed in other amorphous polymer:$PC_{70}BM$ systems.[2,13,42]

Moreover, when exploring the decisive factors affecting the efficiencies of PSCs we must consider not only the


Figure 8. J−V characteristics of PSCs incorporating **P4**:$PC_{70}BM$ blends prepared at various weight ratios (w/w).

Table 4. Photovoltaic Properties of Polymer Solar Cells Incorporating P4:$PC_{70}BM$ Blends Prepared at Various Weight Ratios

P4:$PC_{70}BM$ (w/w)	thickness (nm)	V_{oc} (V)	J_{sc} (mA cm^{-2})	FF	PCE (%)
1:1	84	0.63	7.01	33.3	1.47
1:2	80	0.63	9.16	42.1	2.43
1:3	78	0.62	9.92	43.6	2.68
1:4	75	0.63	10.85	46.1	3.15

absorption and energy levels of polymers but also the surface morphologies of the polymer blends.[53,54] Figure 9 displays the surface morphologies determined through AFM measurements. Samples of the **P1−P4**:$PC_{70}BM$ blends were prepared using procedures identical to those used to fabricate the active layers of the devices. In each case, we observed coarse phase separation in the images of the polymer blends, except for the **P4** blend, which displayed a moderately homogeneous morphology. The **P1** and **P2** blends feature somewhat larger domains than those of the **P3** and **P4** blends; the root-mean-square roughness of the former pair were 4.06 and 8.05 nm, respectively, significantly larger than those of the latter pair (3.50 and 1.53 nm, respectively). The greater phase segregation and rougher surfaces of the **P1** and **P2** blends presumably arose because of poor miscibility with $PCp_{70}BM$—a result of the greater numbers of alkyl groups on the repeat units in these polymer chains.[55,56] This phenomenon was further confirmed by their respective TEM images. Figure 10 shows the TEM images of **P1−P4**:$PC_{70}BM$ blends, where the aggregated $PC_{70}BM$ size in the **P2** blend is in the range of 200−500 nm and is significantly larger than that in the **P4** blend (ca. 70 nm), indicating the relatively better miscibility between **P4** and $PC_{70}BM$ because of the smaller number of alkyl chains. A similar phenomenon was also observed for comparing **P1** with **P3** blends; the aggregated $PC_{70}BM$ size in **P1** was larger than that in **P3**. Accordingly, we suspect that the miscibility of the **P3** and **P4** blends increased after the incorporation of their corresponding thiophene and bithiophene segments because of the reduced number of alkyl groups in the backbone. The AFM and TEM images clearly reveal that the **P4** blend was more homogeneous and smoother than the other three; therefore, its device provided the highest photocurrent. We suggested that the lower power conversion efficiencies of **P1** and **P2** based heterojunction devices as compared to that of **P3** and **P4** based devices result from not only their narrower absorption region but more likely from the phase separation within the blends, as demonstrated by relatively larger $PC_{70}BM$ aggregations in the **P1** and **P2** blends. Even though a few BDT[37] or CPDT[39] based polymers have demonstrated higher devices' power conversion efficiencies, we have used a
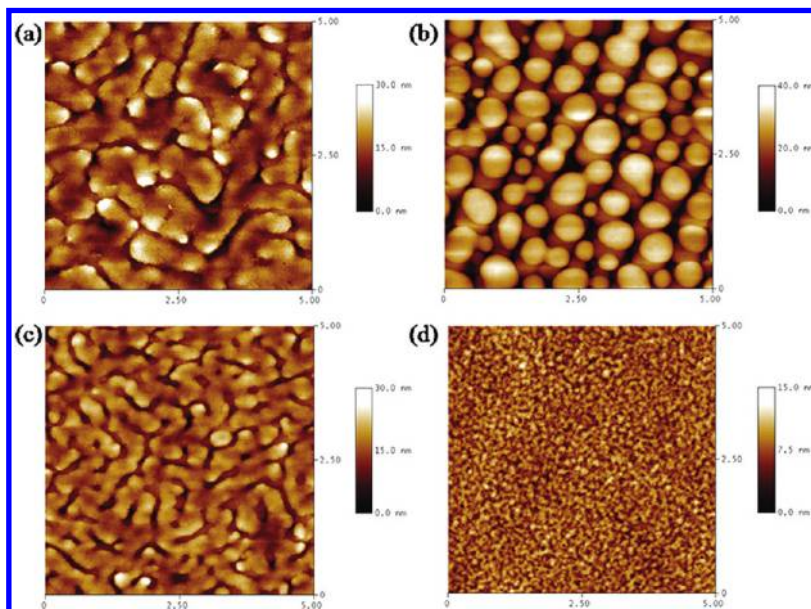
Figure 9. Topographic AFM images of copolymer:PC$_{70}$BM (1:4, w/w) blends incorporating (a) **P1**, (b) **P2**, (c) **P3**, and (d) **P4**.
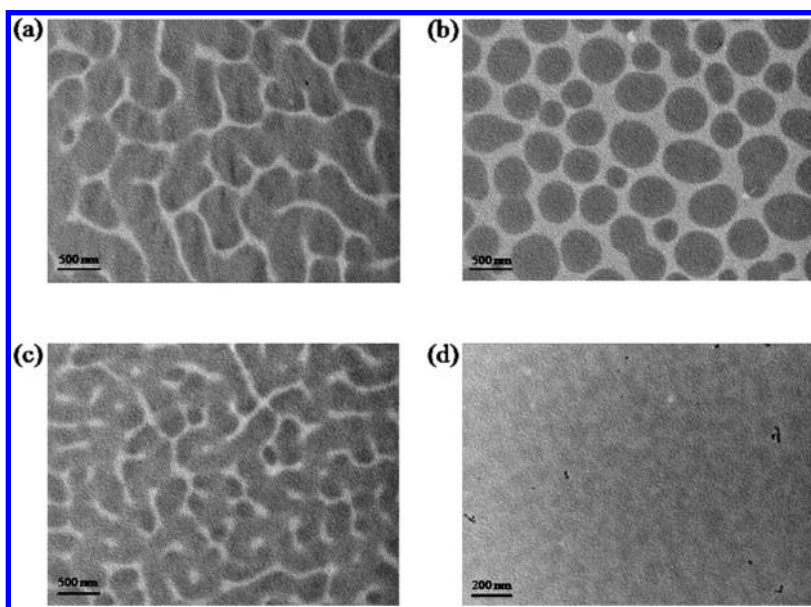
Figure 10. TEM images of copolymer:PC$_{70}$BM (1:4, w/w) blends incorporating (a) **P1**, (b) **P2**, (c) **P3**, and (d) **P4**.

different acceptor, **PP**, for our synthesized polymers; the differences in the intrinsic physical/electronic properties and the blend morphology between our **PP** based polymers and the BDT or CPDT based polymers result in different device's power conversion efficiencies.

Conclusion

We have prepared a series of new pyrido[3,4-*b*]pyrazine (**PP**)-based low-bandgap copolymers conjugated with electron-donating benzo[1,2-*b*:3,4-*b'*]dithiophene (**BDT**) and/or cyclopentadithiophene (**CPDT**) units. The absorption spectra, bandgaps, and energy levels of the polymers can be tuned by using the two different donors, which exhibit different electron-donating abilities. Because the **CPDT** unit exhibited higher electron-donating ability relative to that of the **BDT** unit, its presence resulted in stronger ICT interactions when conjugated with **PP** moieties. Therefore, the absorptions of the **CPDT**-containing polymers were significantly red-shifted relative to those of the **BDT**-containing

polymers. Moreover, **P3** and **P4** absorbed broadly, covering the solar spectrum from the visible to the NIR, because of the presence of the thiophene/bithiophene segments in their polymer backbones; accordingly, their corresponding devices functioned with improved photocurrents. Furthermore, among our four tested polymer blends, the **P4** blend possessed the most homogeneous surface, presumably contributing to its more efficient carrier transport and dissociation. As a result, the best device performance was obtained when using the **P4**:PC$_{70}$BM blend, characterized by a high short-circuit current of 10.85 mA cm^{-2} and a resulting PCE of 3.15%.

Supporting Information Available: Figures showing ^{1}H NMR spectra of the synthesized polymers. This material is available free of charge via the Internet at http://pubs.acs.org.

References and Notes

(1) Yu, G.; Gao, J.; Hummelen, J. C.; Wudl, F.; Heeger, A. J. *Science* **1995**, *270*, 1789.

(2) Wienk, M. M.; Kroon, J. M.; Verhees, W. J. H.; Knol, J.; Hummelen, J. C.; van Hal, P. A.; Janssen, R. A. J. *Angew. Chem., Int. Ed.* **2003**, *42*, 3371.

(3) Hoppe, H.; Niggemann, M.; Winder, C.; Kraut, J.; Hiesgen, R.; Hinsch, A.; Meissner, D.; Sariciftci, N. S. *Adv. Funct. Mater.* **2004**, *14*, 1005.

(4) Günes, S.; Neugebauer, H.; Sariciftci, N. S. *Chem. Rev.* **2007**, *107*, 1324.

(5) Ma, W.; Yang, C.; Gong, X.; Lee, K.; Heeger, A. J. *Adv. Funct. Mater.* **2005**, *15*, 1617.

(6) Li, G.; Shrotriya, V.; Huang, J.; Yao, Y.; Moriarty, T.; Emery, K.; Yang, Y. *Nat. Mater.* **2005**, *4*, 864.

(7) Kim, Y.; Cook, S.; Tuladhar, S. M.; Choulis, S. A.; Nelson, J.; Durrant, J. R.; Bradley, D. D. C.; Giles, M.; McCulloch, I.; Ha, C.-S.; Ree, M. *Nat. Mater.* **2006**, *5*, 197.

(8) Chiu, M.-Y.; Jeng, U.-S.; Su, C.-H.; Liang, K. S.; Wei, K.-H. *Adv. Mater.* **2008**, *20*, 2573.

(9) Bundgaard, E.; Krebs, F. C. *Sol. Energy Mater. Sol. Cells* **2007**, *91*, 954.

(10) Huo, L. J.; Tan, Z.; Wang, X.; Zhou, Y.; Han, M. F.; Li, Y. F. *J. Polym. Sci., Part A: Polym. Chem.* **2008**, *46*, 4038.

(11) Xin, H.; Guo, X.; Kim, F. S.; Ren, G.; Watson, M. D.; Jenekhe, S. A. *J. Mater. Chem.* **2009**, *19*, 5303.

(12) Zhou, E.; Yamakawa, S.; Tajima, K.; Yang, C.; Hashimoto, K. *Chem. Mater.* **2009**, *21*, 4055.

(13) Lindgren, L. J.; Zhang, F.; Andersson, M.; Barrau, S.; Hellström, S.; Mammo, W.; Perzon, E.; Inganäs, O.; Andersson, M. R. *Chem. Mater.* **2009**, *21*, 3491.

(14) Qin, R.; Li, W.; Li, C.; Du, C.; Veit, C.; Schleiermacher, H.-F.; Andersson, M.; Bo, Z.; Liu, Z.; Inganäs, O.; Wuerfel, U.; Zhang, F. *J. Am. Chem. Soc.* **2009**, *131*, 14612.

(15) Chang, Y.-T.; Hsu, S.-L.; Su, M.-H.; Wei, K.-H. *Adv. Funct. Mater.* **2007**, *17*, 3326.

(16) Chang, Y.-T.; Hsu, S.-L.; Chen, G.-Y.; Su, M.-H.; Singh, T. A.; Diau, E. W.-G.; Wei, K.-H. *Adv. Funct. Mater.* **2008**, *18*, 2356.

(17) Chang, Y.-T.; Hsu, S.-L.; Su, M.-H.; Wei, K.-H. *Adv. Mater.* **2009**, *21*, 2093.

(18) Huang, F.; Chen, K.-S.; Yip, H.-L.; Hau, S. K.; Acton, O.; Zhang, Y.; Luo, J.; Jen, A. K.-Y. *J. Am. Chem. Soc.* **2009**, *131*, 13886.

(19) Yuan, M.-C.; Su, M.-H.; Chiu, M.-Y.; Wei, K.-H. *J. Polym. Sci., Part A: Polym. Chem.* **2010**, *48*, 1298.

(20) Huo, L.; Hou, J.; Chen, H.-Y.; Zhang, S.; Jiang, Y.; Chen, T. L.; Yang, Y. *Macromolecules* **2009**, *42*, 6564.

(21) Liang, Y.; Wu, Y.; Feng, D.; Tsai, S.-T.; Son, H.-J.; Li, G.; Yu, L. *J. Am. Chem. Soc.* **2009**, *131*, 56.

(22) Mondal, R.; Miyaki, N.; Becerril, H. A.; Norton, J. E.; Parmer, J.; Mayer, A. C.; Tang, M. L.; Brédas, J.-L.; McGehee, M. D.; Bao, Z. *Chem. Mater.* **2009**, *21*, 3618.

(23) Zhou, E.; Wei, Q.; Yamakawa, S.; Zhang, Y.; Tajima, K.; Yang, C.; Hashimoto, K. *Macromolecules* **2010**, *43*, 821.

(24) Zhou, H.; Yang, L.; Xiao, S.; Liu, S.; You, W. *Macromolecules* **2010**, *43*, 811.

(25) Chen, G.-Y.; Chiang, C.-M.; Kekuda, D.; Lan, S.-C.; Chu, C.-W.; Wei, K.-H. *J. Polym. Sci., Part A: Polym. Chem.* **2010**, *48*, 1669.

(26) Yamamoto, T.; Zhou, Z.-H.; Kanbara, T.; Shimura, M.; Kizu, K.; Maruyma, T.; Nakamura, Y.; Fukuda, T.; Lee, B.-L.; Ooba, N.; Tomaru, S.; Kurihara, T.; Kaino, T.; Kubota, K.; Sasaki, S. *J. Am. Chem. Soc.* **1996**, *118*, 10389.

(27) Lee, B.-L.; Yamamoto, T. *Macromolecules* **1999**, *32*, 1375.

(28) Jonforsen, M.; Johansson, T.; Inganäs, O.; Andersson, M. R. *Macromolecules* **2002**, *35*, 1638.

(29) Jonforsen, M.; Johansson, T.; Spjuth, L.; Inganäs, O.; Andersson, M. R. *Synth. Met.* **2002**, *131*, 53.

(30) Thompson, B. C.; Madrigal, L. G.; Pinto, M. R.; Kang, T.-S.; Schanze, K. S.; Reynolds, J. R. *J. Polym. Sci., Part A: Polym. Chem.* **2005**, *43*, 1417.

(31) Wu, P.-T.; Kim, F. S.; Champion, R. D.; Jenekhe, S. A. *Macromolecules* **2008**, *41*, 7021.

(32) Jonforsen, M.; Ahmad, I.; Johansson, T.; Larsson, J.; Roman, L. S.; Svensson, M.; Inganäs, O.; Andersson, M. R. *Synth. Met.* **2001**, *119*, 185.

(33) Zhang, F.; Jonforsen, M.; Johansson, D. M.; Andersson, M. R.; Inganäs, O. *Synth. Met.* **2003**, *138*, 555.

(34) Blouin, N.; Michaud, A.; Gendron, D.; Wakim, S.; Blair, E.; Neagu-Plesu, R.; Belletête, M.; Durocher, G.; Tao, Y.; Leclerc, M. *J. Am. Chem. Soc.* **2008**, *130*, 732.

(35) Wu, P.-T.; Bull, T.; Kim, F. S.; Luscombe, C. K.; Jenekhe, S. A. *Macromolecules* **2009**, *42*, 671.

(36) Hou, J.; Park, M.-H.; Zhang, S.; Yao, Y.; Chen, L.-M.; Li, J.-H.; Yang, Y. *Macromolecules* **2008**, *41*, 6012.

(37) Chen, H.-Y.; Hou, J.; Zhang, S.; Liang, Y.; Yang, G.; Yang, Y.; Yu, L.; Wu, Y.; Li, G. *Nat. Photonics* **2009**, *3*, 649.

(38) Zhu, Z.; Waller, D.; Gaudiana, R.; Morana, M.; Mühlbacher, D.; Scharber, M.; Brabec, C. J. *Macromolecules* **2007**, *40*, 1981.

(39) Lee, J. K.; Ma, W. L.; Brabec, C. J.; Yuen, J.; Moon, J. S.; Kim, J. Y.; Lee, K.; Bazan, G. C.; Heeger, A. J. *J. Am. Chem. Soc.* **2008**, *130*, 3619.

(40) Bijleveld, J. C.; Shahid, M.; Gilot, J.; Wienk, M. M.; Janssen, R. A. J. *Adv. Funct. Mater.* **2009**, *19*, 3262.

(41) Li, K.-C.; Huang, J.-H.; Hsu, Y.-C.; Huang, P.-J.; Chu, C.-W.; Lin, J.-T.; Ho, K.-C.; Wei, K.-H.; Lin, H.-C. *Macromolecules* **2009**, *42*, 3681.

(42) Gadisa, A.; Mammo, W.; Andersson, L. M.; Admassie, S.; Zhang, F.; Andersson, M. R.; Inganäs, O. *Adv. Funct. Mater.* **2007**, *17*, 3836.

(43) Melzer, C.; Koop, E. J.; Mihailetchi, V. D.; Blom, P. W. M. *Adv. Funct. Mater.* **2004**, *14*, 865.

(44) Chaloner, P. A.; Gunatunga, S. R.; Hitchcock, P. B. *J. Chem. Soc., Perkin Trans. 2* **1997**, 1597.

(45) Jung, Y. K.; Kim, H.; Park, J.-H.; Lee, J.; Lee, S. K.; Lee, Y. S.; Shim, H.-K. *J. Polym. Sci., Part A: Polym. Chem.* **2008**, *46*, 3573.

(46) Ajayaghosh, A. *Chem. Soc. Rev.* **2003**, *32*, 181.

(47) Zhu, Y.; Champion, R. D.; Jenekhe, S. A. *Macromolecules* **2006**, *39*, 8712.

(48) Pommerehne, J.; Vestweber, H.; Guss, W.; Mahrt, R. F.; Bässler, H.; Porsch, M.; Daub, J. *Adv. Mater.* **1995**, *7*, 551.

(49) Brédas, J.-L.; Beljonne, D.; Coropceanu, V.; Cornil, J. *Chem. Rev.* **2004**, *104*, 4971.

(50) Thompson, B. C.; Fréchet, J. M. J. *Angew. Chem., Int. Ed.* **2008**, *47*, 58–77.

(51) Scharber, M. C.; Mühlbacher, D.; Koppe, M.; Denk, P.; Waldauf, C.; Heeger, A. J.; Brabec, C. J. *Adv. Mater.* **2006**, *18*, 789.

(52) Pal, B.; Yen, W.-C.; Yang, J.-S.; Chao, C.-Y.; Hung, Y.-C.; Lin, S.-T.; Chuang, C.-H.; Chen, C.-W.; Su, W.-F. *Macromolecules* **2008**, *41*, 6664.

(53) Li, G.; Yao, Y.; Yang, H.; Shrotriya, V.; Yang, G.; Yang, Y. *Adv. Funct. Mater.* **2007**, *17*, 1636.

(54) Hoppe, H.; Sariciftci, N. S. *J. Mater. Chem.* **2006**, *16*, 45.

(55) Liang, Y.; Feng, D.; Wu, Y.; Tsai, S.-T.; Li, G.; Ray, C.; Yu, L. *J. Am. Chem. Soc.* **2009**, *131*, 7792.

(56) Lai, M.-H.; Chueh, C.-C.; Chen, W.-C.; Wu, J.-L.; Chen, F.-C. *J. Polym. Sci., Part A: Polym. Chem.* **2009**, *47*, 973.